



The spectrum of fault slip in elastoplastic fault zones

Md Shumon Mia ^{a,b,*}, Mohamed Abdelmeguid ^{b,c}, Ahmed E. Elbanna ^{b,d}



^a Department of Mechanical Science and Engineering, University of Illinois at Urbana-Champaign, Urbana, IL, USA

^b Department of Civil and Environmental Engineering, University of Illinois at Urbana-Champaign, Urbana, IL, USA

^c Graduate Aerospace Laboratories, California Institute of Technology, Pasadena, CA, USA

^d Beckman Institute of Advanced Science and Technology, University of Illinois at Urbana-Champaign, Urbana, IL, USA

ARTICLE INFO

Article history:

Received 11 March 2023

Received in revised form 27 June 2023

Accepted 8 July 2023

Available online 26 July 2023

Editor: R. Bendick

Dataset link: <https://doi.org/10.5281/zenodo.7718768>

Keywords:

earthquake cycle
slow slip
off-fault deformation
numerical simulation
plasticity
fault zones

ABSTRACT

Natural faults are typically surrounded by damage zones that exhibit inelastic material response. This study investigates the role of fault zone strength in modulating the spectrum of fault slip across different spatio-temporal scales. We carry out long-term simulations of seismic and aseismic slip for an elastoplastic spring slider model with rate-and-state friction as well as a continuum model of a 2D anti-plane rate-and-state fault embedded in an elastoplastic bulk. Results of the elastoplastic spring slider model show the emergence of a new stability boundary, depending on the bulk yield strength relative to fault frictional strength, that limits the rupture size regardless of the fault length. Continuum simulations generate a spectrum of slip analogous to the spring slider model including localized or migrating events of slow and fast slip. A fault may remain locked for yield strength sufficiently low and close to fault reference strength even if it is intrinsically rate weakening and larger than the nucleation length scale predicted by the elastic analysis. These findings shed new light on the nature of fault frictional stability and suggest the critical role of the fault zone rheological properties in modulating the spectrum of fault slip.

© 2023 Elsevier B.V. All rights reserved.

1. Introduction

Unstable sliding of geologic faults manifests itself as earthquakes—one of the deadliest and most prevalent yet unpredictable natural hazards. Apart from large earthquakes, faults are also found to host small earthquakes and slow slip events (Beroza and Ide, 2011; Ito et al., 2013; Bürgmann, 2018). Usually, earthquakes are associated with frictional sliding on fault surfaces encompassing long-term slow aseismic slip and rapid seismic ruptures (Avouac, 2015). However, fault zone complexities, including geometric and material non-linearity (Ben-Zion and Sammis, 2003; Mitchell and Faulkner, 2009; Lewis and Ben-Zion, 2010), influence the fault slip behavior leading to complex patterns of seismicity in space and time (Chen et al., 2020; Ross et al., 2020). Physics-based simulations for sequences of earthquakes and aseismic slip (Ben-Zion and Rice, 1993; Lapusta et al., 2000; Chen and Lapusta, 2009; Kaneko et al., 2010; Barbot et al., 2012; Allison and Dunham, 2021; Erickson et al., 2023; Jiang et al., 2022; Abdelmeguid and Elbanna, 2022a, 2022b) are emerging as promising tools for understanding the complex processes associated with different forms of frictional

instabilities and resulting slip pattern, as well as in developing seismic hazard models.

Stable and unstable frictional sliding is largely attributed to the frictional properties of the fault whether the steady-state frictional strength increases with slip rate (velocity strengthening) or decreases with slip rate (velocity weakening). A velocity-strengthening patch is generally associated with stable aseismic sliding and may become unstable through enhanced coseismic weakening associated with flash heating or a rapid increase in pore fluid pressure due to shear heating (Noda and Lapusta, 2013). While a fault with velocity-weakening friction is locked during the interseismic period, it is potentially unstable and generates different patterns of slip. The style of slip in terms of peak slip rate, spatial extent, and temporal periodicity, depends on the size of the velocity weakening patch relative to the critical length scale associated with nucleation as well as the relative magnitude of frictional parameters associated with static and dynamic stress drop (Barbot, 2019; Cattania, 2019). Generation of slow slip sequence accompanied by slow earthquakes are shown in Barbot (2019) to depend on the relative magnitude of the frictional parameters and the relative fault size. Specifically, slow slip is found in these studies when the length of the velocity weakening patch is close to the nucleation length.

* Corresponding author at: Department of Mechanical Science and Engineering, University of Illinois at Urbana-Champaign, Urbana, IL, USA.

E-mail address: mnia2@illinois.edu (M.S. Mia).

Experimental studies (Leeman et al., 2016; Scuderi et al., 2016) show emergence of spectrum of slip controlled by the ratio between the elastic stiffness (k) of the loading medium and the critical stiffness (k_c) governed by frictional rheology. Stable sliding corresponds to $\frac{k}{k_c} > 1$ and fast stick-slip instability occurs with $\frac{k}{k_c} \ll 1$. Slow slip is observed near the transition between stable and unstable sliding with $\frac{k}{k_c} \sim 1$. These results conform with the stability analysis of spring slider model with rate-and-state friction (Ranjith and Rice, 1999) and provide a possible explanation for the spectrum of fault slip considering the off-fault bulk as elastic.

Geologic heterogeneities observed along natural faults (Fagereng and Sibson, 2010; Collettini et al., 2019) can play a role in generating different styles of slip including slow slip and fast rupture. Skarbek et al. (2012) shows that geologic heterogeneity in terms of the different proportions of velocity strengthening and velocity weakening patches may give rise to slow slip. Small scale heterogeneity in fault gauge inferred from laboratory friction experiment (Bedford et al., 2022) is shown to influence frictional stability through reduction in fault strength with increased heterogeneity. Also, the rate-dependent evolution (Kaproth and Marone, 2013) of frictional parameters is a possible mechanism for slow slip generation. Velocity-weakening friction generating stick-slip instabilities may generate slow slip when rate-and-state friction parameters evolve with slip rate and take transition from velocity weaking to velocity strengthening. Numerical simulations using a spring-slider model by Im et al. (2020) show that velocity dependent frictional parameters enable generating slow slip events having similar characteristics to those observed in nature (Dragert et al., 2001; Heki and Kataoka, 2008; Radiguet et al., 2012). However, it is not clear what physical mechanism may lead to this rate dependence of the frictional parameters.

Pore pressure also plays an important role in controlling spectrum of slip. Fluid pressure reduces effective normal stress and increases the nucleation length scale. Accordingly, the size of the seismogenic velocity-weakening patch decreases relative to the size of the nucleation patch. This results in slow slip transients (Liu and Rice, 2007). Dilatant strengthening (Segall et al., 2010), resulting in reduced pore pressure, also explains the generation of slow slip events in a seismogenic velocity-weakening region. Slow and fast slip may arise through the relative contribution of dilatancy-induced strengthening and enhanced coseismic weakening due to thermal pressurization of pore fluid. Dilatant hardening itself may be a manifestation of inelastic processes associated with propagating crack tip (French and Zhu, 2017).

These on-fault characteristics controlling the spectrum of slip are investigated mostly with homogeneous elastic bulk. Heterogeneous bulk with a low velocity zone near the fault may generate slip complexity (Abdelmeguid et al., 2019; Thakur et al., 2020; Nie and Barbot, 2022). Also, a recent study by Collettini et al. (2022) explains the observation of distributed microseismicity through a conceptual model of distributed ductile deformation in the bulk. Incorporation of viscoelastic fault zones (Miyake and Noda, 2019; Goswami and Barbot, 2018) and viscous damping in fault strength (Wu, 2021; Nakata et al., 2011) are shown to generate slow slip events. Erickson et al. (2017) models earthquake cycle in rate-and-state fault with off-fault plasticity. They show partitioning of deformation and resulting slip deficit with off-fault plasticity accumulation near the free surface of a vertical fault. However, the resulting pattern of seismicity with off-fault plasticity is similar, in their study, to the homogeneous elastic case having periodic seismic events. Using numerical simulation with elastoplastic shear zone, Tong and Lavie (2018) shows generation of slow and fast slip events by varying the rate-and-state friction parameters. By reducing the difference between the direct effect parameter and state evolution parameter, they found slip pattern to change from

fast slip events to slow slip. In the limit of vanishing difference between the friction parameters, corresponding to the limit of velocity neutral, creeping events are found.

In our previous work on seismic cycle simulations with off-fault plasticity (Mia et al., 2022), we showed that bulk yield strength and post-yield viscous relaxation contribute to the emergence of spatio-temporal clustering of seismicity. Here, we investigate the effect of off-fault bulk strength on fault slip expanding the parameter space for yield strength to also consider values close to the reference frictional strength. This is a critical parameter regime that have not been investigated before and may qualitatively alter the partitioning of slip and energy dissipation between on-fault and off-fault processes. To that end, we first simulate the long-term frictional sliding of an elastoplastic spring slider model with rate-and-state friction. Then, to further corroborate our findings, we investigate sequences of seismic and aseismic slip on a 2D anti-plane rate and state model embedded in a fully continuum elastoplastic model. We evaluate the resulting slip patterns with a special focus on slow slip.

2. Elastoplastic spring slider

We simulate the long-term sliding of a spring-block system under constant load-point velocity applied at the end of the spring. The details of the spring slider model are outlined in the Supplementary Information (Figure-S1, Text-S2). The spring with stiffness (k) and yield strength (σ_y) idealize the bulk material with elastoplastic response. The frictional interface represents a fault surface with uniform friction. The friction here is velocity weakening governed by rate-and-state friction law (Dieterich, 1979; Ruina, 1983) and the state evolution follows the aging law (Dieterich, 1978; Ruina, 1983; Ben-Zion and Rice, 1997; Ampuero and Rubin, 2008). The friction law is outlined in the Supplementary Information (Text-S1). To investigate the effect of bulk strength on frictional sliding, we vary the yield strength (σ_y) and the stiffness (k) of the spring. Critical stiffness (Rice and Ruina, 1983; Ranjith and Rice, 1999) is related to the frictional properties and normal stress (σ_n), and is defined by, $k_{cr} = \sigma_n(b - a)/L$. Where, a , and b are non-negative dimensionless parameters associated with rate-and-state friction law. At steady state, $(b - a)$ defines the velocity dependence of friction coefficient with $(b - a) > 0$ indicates that steady-state friction decreases with the increase in the sliding velocity, i.e., velocity-weakening response. L is the characteristic slip distance. Critical stiffness marks the transition between stable and unstable frictional sliding in a purely elastic setting.

From stability analysis (Ranjith and Rice, 1999; Rice et al., 2001), it is known that stiffness greater than the critical value corresponds to stable sliding which tends to attain steady state in sync with the imposed load point velocity. For elastic spring, stiffness lower than the critical value generates unstable sliding. The elastoplastic spring block slider shows different sliding patterns ranging from stick-slip to complete locking depending on the yield strength and the elastic stiffness of the spring (Fig. 1). The slip rate vs. time plots for selected values of yield strength and spring stiffness are presented in Fig. 2. We classify the slip patterns based on the amplitude of the block's peak slip rate (Goswami and Barbot, 2018; Tong and Lavie, 2018; Miyake and Noda, 2019). Slow slip is identified with slip rate lower than a seismic threshold (taken here to be 0.01 m/s) but higher than the background plate rate (10^{-9} m/s). Stick slip corresponds to slip rate exceeding the seismic threshold. We observe that slow slip emerges for a narrow range of yield strength and stiffness values (Fig. 1). The block also creeps stably at the imposed loading rate for stiffness values larger than the critical value predicted by the elastic analysis. However, as shown in Fig. 1, another new transition boundary emerges with plasticity, in the limit of lower stiffness, that is not

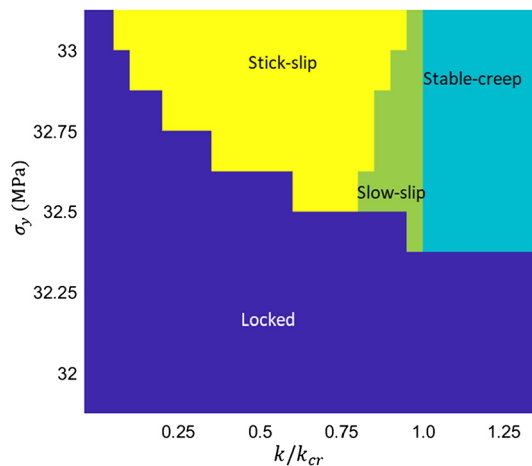


Fig. 1. Sliding patterns for an elastoplastic spring block system depending on yield strength (σ_y) and stiffness (k) of the spring. Reference strength of the frictional interface is $\sigma_n f_0 = 30$ MPa. Sliding patterns change from stick-slip to slow-slip as spring stiffness becomes close to a critical stiffness defined for the elastic system from the frictional parameters as $k_{cr} = \sigma_n(b-a)/L$. For stiffness higher than critical value, the sliding is stable. A region of slow-slip exists between stick-slip and stable-creep for a narrow range of stiffness and yield strength values. There is another transition towards lower stiffness, which depends on the magnitude of the yield strength, where the slider remains locked. This new stability boundary does not exist for purely elastic spring block systems.

observed in purely elastic analysis. This transition from stick-slip to locking (i.e., sliding with slip rates that are orders of magnitudes slower than the imposed plate loading rate) depends on the yield strength. As yield strength decreases, this transition stiffness increases. For sufficiently low yield strength, as it becomes close to the reference frictional strength ($\sigma_n f_0$), the slip rate asymptotically decreases to $\sim 10^{-15}$ m/s, orders of magnitude lower than the imposed plate rate. We refer to the sliding with this negligible slip rate as locked.

3. Continuum simulation of a 2D anti-plane rate-and-state fault

We model a 2D anti-plane rate-and-state fault embedded in a full-space elastoplastic medium subjected to slow tectonic plate rate. The fault has a central velocity-weakening (VW) region surrounded by velocity-strengthening (VS) patches from both sides (Supplementary Figure-S2). The length of the VW patch is around 5 times the nucleation length. We model off-fault material response with J2 plasticity which coincides with Drucker-Prager plasticity for the anti-plane setting with no variations in normal stress. We further assume no plastic hardening. In this study, we consider the elastoplastic response as a proxy for isotropic microscale damage. While damage processes may also produce time-dependent changes in the elastic moduli through degradation and healing, as well as anisotropic material response, we ignore these changes in this study. We elaborate on this approximation in the discussion section. A hybrid scheme combining finite element and spectral boundary integral is employed for spatial discretization (Abdelmeguid et al., 2019; Mia et al., 2022; Abdelmeguid and Elbanna, 2022b). We use an adaptive time-stepping algorithm (Lapusta et al., 2000) to efficiently resolve slow and fast slip. The model geometry with the hybrid scheme setup as well as the input parameters for the simulations are outlined in the Supplementary Information (Text-S3, Table-S1, Figure-S2).

We simulate sequences of earthquakes and aseismic slip (SEAS) with different values of yield strength to investigate the effect of bulk strength on long-term fast and slow slip. Resulting patterns, given as space-time contours of the fault slip rate, with different values of yield strength are shown in Fig. 3. The temporal evolution

of the peak slip rate in different cases is shown in Fig. 4. The simulations show sliding patterns analogous to the elastoplastic spring slider model. For lower yield strength the fault remains locked without generating any seismic event. When the yield strength is increased, the fault generates unstable frictional sliding including slow slip, spatially localized seismic events, and partial ruptures distributed over the fault length intermixed with transient episodes of slow slip. For higher values of yield strength, or in the limit of purely elastic bulk, the fault fails in predominantly large, fault-spanning, fast earthquakes. Below we briefly describe these different slip regimes.

Locked fault: When the yield strength (31 MPa) is close to the fault reference frictional strength ($\sigma_n f_0 = 30$ MPa), the slip rate of the central VW patch decreases to $\sim 10^{-15}$ m/s (Fig. 3a). The instantaneous and steady-state frictional strength for such low slip rate is higher than the reference frictional strength. Relative to the plate loading rate, this slip rate is orders of magnitude smaller which indicates that the seismogenic zone (VW patch) of the fault remains effectively locked or stuck. The VS patch of the fault creeps following the plate loading. Aseismic creep from the VS patch penetrates slightly into the VW patch but the peak slip rate remains close to the imposed plate rate (10^{-9} m/s) in a very limited region adjacent to the VS patch as shown in Fig. 3a and Fig. 4a.

Slow slip: When the yield strength is increased to 32 MPa, slow slip emerges (Fig. 3b, 3g, 3j). Signature of creep penetration exists near the transition between the VS and VW patches. The duration of the slow slip events for yield strength 32 MPa is in the scale of weeks to month. Spatially, these events are localized near the transition region from VS to VW. Similar spatially localized slow slip events are also observed in between localized partial ruptures for yield strength 32.5 MPa (Fig. 3c, 3h, 3k). However, the peak slip rate associated with some of these aseismic transients reaches orders of magnitude higher than the background plate rate. The irregular pattern with yield strength 33.5 MPa also includes slow slip events (Fig. 3d, 3i, 3l). The peak slip rates associated with these slow slip events are even higher, but they are still below the seismic threshold. These slow slip events, observed with yield strength 33.5 MPa, are no longer localized in the transition region. Rather they show spatial migration over the full length of the seismogenic (Velocity-Weakening) patch of the fault.

Localized seismic events: A repeating pattern of localized seismic events is observed for yield strength 32.5 MPa as shown in Fig. 3c. These seismic events are inter-mixed with slow slip episodes as described above. The seismic events are spatially localized near the boundary between VS and VW. They rupture approximately the same area, but they do not repeat with the exact return period (Fig. 4c). Their average stress drop is around 2.3 MPa with standard deviation of 0.5 MPa approximately which is consistent with stress drop measured for earthquake repeaters (Chen and Lapusta, 2009). The slow slip events observed in this case occur mostly before the seismic events.

Stick-slip with partial ruptures: When yield strength is increased to 33.5 MPa, fault sliding includes slow slip and partial seismic ruptures (Fig. 3d). In the early stages of the sequence, partial ruptures extend on both sides of fault, but a locked patch remains in the center that gets progressively narrower with time. Later in the cycle, the whole VW region is ruptured by subsequent partial events. Here the partial ruptures are prevalent throughout the VW patch unlike the localized repeating events shown in Fig. 3b. Also, the clustering of events observed with relatively higher yield strength e.g., 36 MPa (Figure-3e) is not found for the case with yield strength 33.5 MPa.

Stick-slip with fault-spanning ruptures: For relatively higher yield strength (e.g., 36 MPa shown in Fig. 3e), seismic events, including partial ruptures as well as ruptures spanning the full VW

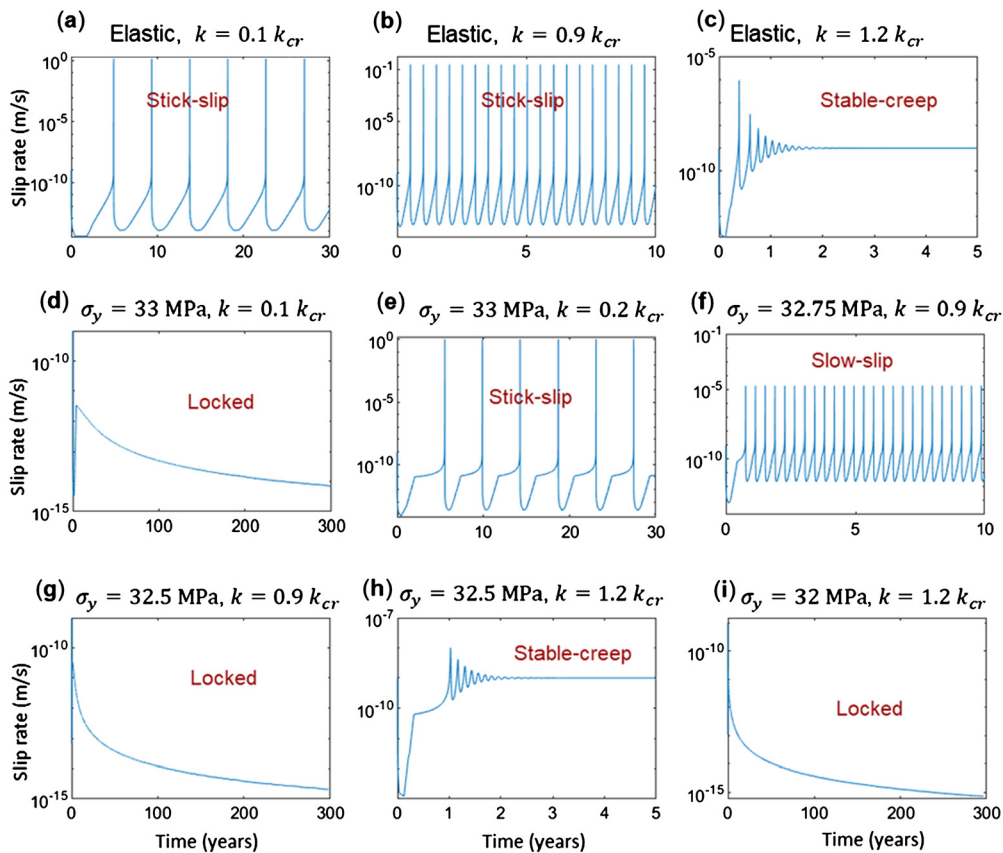


Fig. 2. History of slip rate demonstrating various sliding patterns for the spring slider model with different values of yield strength (σ_y) and elastic stiffness (k). The elastic case (shown in a-c.) corresponds to stability transition from stick-slip to stable-creep when stiffness exceeds a critical value ($k > k_{cr}$). For stick-slip instability, slip rate exceeds a seismic threshold (taken 0.01 m/s here), and for stable-creep, slip rate decays to applied plate rate (10^{-9} m/s). For the elastoplastic spring (shown in d-i), another stability transition appears depending on the magnitude of yield strength where the slider remains locked (shown in d, g, i) as the slip rate is several orders of magnitude lower than the plate rate. Slip rate lower than the seismic threshold but greater than plate rate corresponds to slow slip as shown in f.

patch, dominate the slip pattern. Evolution of the spatial extent of rupture, discussed above for lower yield strength, showing central locked patches progressively unclamped with time does not exist with relatively higher yield strength. The resulting sequence, including partial and fault-spanning rupture, is aperiodic with clustering of seismic events in space and time. Simulation with elastic bulk (Fig. 3f) results in simple periodic cycle with fault-spanning ruptures only. Cycle simulations for a range of high values of yield strength and post-yield viscosity are discussed in our previous study (Mia et al., 2022) where seismicity pattern changes from complex spatio-temporal clustering to simple periodic pattern with increasing yield strength and post-yield viscosity. While here we adopted a quasi-dynamic approximation of inertia effect through a radiation damping term, the results are qualitatively similar even if we consider full inertia effects (Supplementary Information, Figure-S3).

Partitioning of deformation

Plasticity results in a slip deficit on the fault surface through partitioning of total deformation into on-fault slip and off-fault plastic deformation. In Fig. 5, the spatial distribution of the cumulative slip and off-fault plastic deformation is shown for yield strength 33.5 MPa. Here we calculate an effective measure for the variation of the plastic deformation in the fault zone along the fault length by integrating the equivalent plastic strain, γ , as $u_p(x, t) = 2 \int_0^{L_y} \gamma(x, y, t) dy$, where, L_y is the half width of the computational strip modeled using FEM, and y represents the spatial direction normal to the fault plane. The factor of 2 accounts for the symmetry of the plastic strain distribution about the fault surface. This is characteristics of anti-plane plasticity in homogeneous

media where the normal stress does not change with deformation. For the current model geometry, $L_y = 30$ m which is around 1.5 times the process zone size. This width is found sufficient to contain the spatial extent of plasticity in the fault normal direction. Outside this computational strip, the exterior half-spaces are elastic and are modeled using the spectral boundary integral approach. Therefore, they do not experience plastic deformation. Total plastic deformation along the fault, $u_p(x, t)$ is shown in Fig. 5b. Cumulative slip is plotted in Fig. 5a. The contour lines for both quantities are plotted every 10 years up to 50 years.

As shown in Fig. 5a, cumulative slip in the VS patch is around 1.5 m in 50 years. Slip accumulation is reduced near the transition from VS to VW and is further reduced in the interior of the locked VW region. The central region of the VW patch is locked in early stages. As time passes, seismic events progressively unlock the VW fault through a sequence of partial ruptures as shown in Fig. 3d. The non-smooth shape of the cumulative slip lines corresponds to the irregular pattern of slow slip and partial ruptures spreading over the whole VW region. From the plastic deformation plot (Fig. 5b), it is evident that plastic deformation in the bulk compensates for the slip deficit in the VW patch. Plastic deformation is maximum in the central part of the VW patch where the fault slip is minimum and gradually vanishes towards the VS region.

Off-fault plastic deformation gets an increasing share of the total deformation budget when the bulk yield strength is lower. To evaluate the partitioning of deformation and associated slip pattern for different values of yield strength, we compute the on-fault deformation by integrating fault slip termed as Potency (t) =

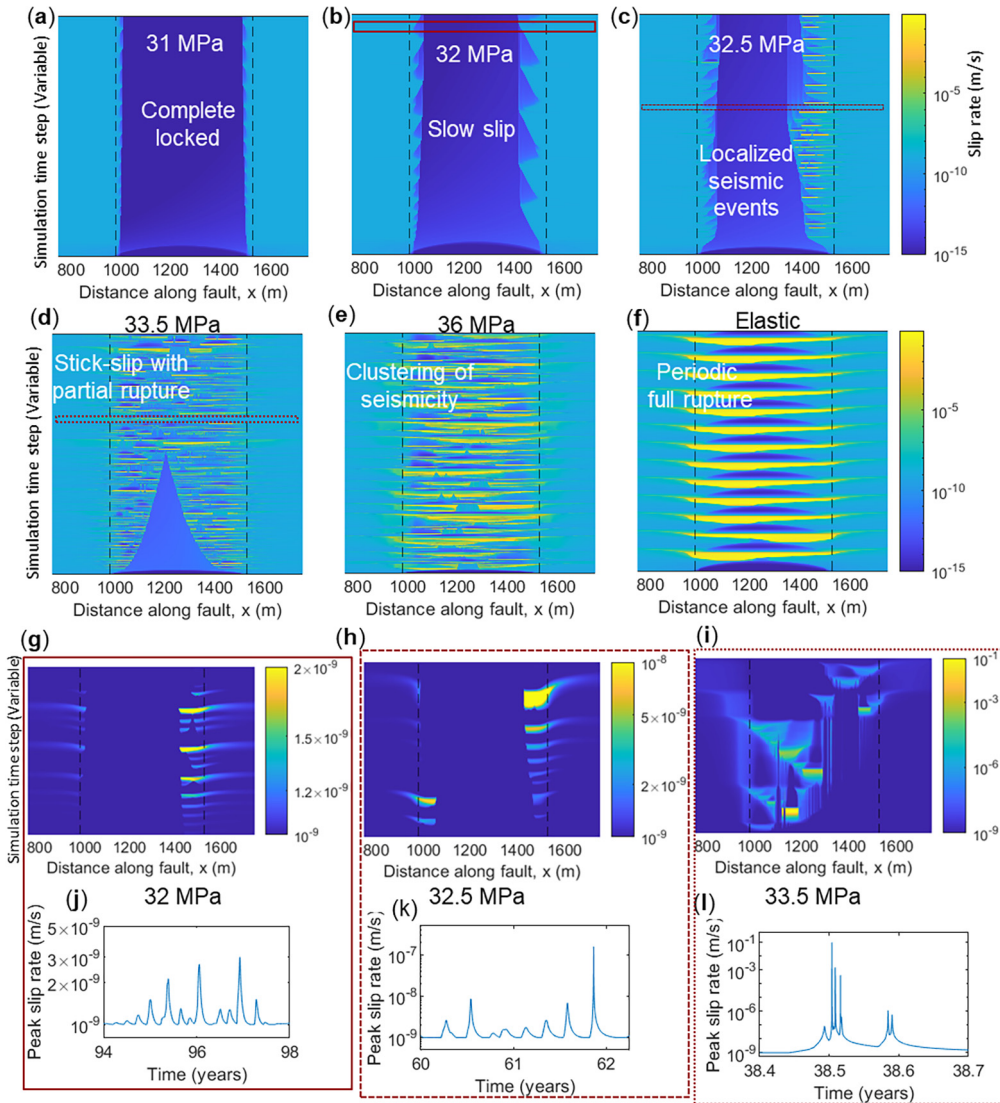


Fig. 3. Spectrum of slip for a rate-and-state fault. Spatio-temporal evolution of slip rate illustrating different slip pattern for different yield strength (a-e). Elastic case results in periodic seismic cycle as shown in f. Region between two vertical dashed lines correspond to velocity weakening friction. Fault reference strength is $\sigma_n f_0 = 30. Fault remains locked for yield strength, $\sigma_y = 31. Locked fault with occasional slow slip is found for $\sigma_y = 32. Localized earthquakes near the transition between VS and VW are shown in c. Complex pattern including slow slip and seismic events with partial rupture is shown in d. Clustering of seismicity is found when yield strength is increased (e). Closer examination of example of slow slip events that exist with $\sigma_y = 32$, 32.5 and 33.5 MPa are shown in g-l.$$$

$\int_0^{L_f} d(x, t) dx$, and off-fault plastic deformation by integrating the equivalent plastic strain over the domain as $PD(t) = \int_S \gamma(x, y, t) dy$. Where d is the slip, L_f is the seismogenic region of the fault including VW patch and the transition region between VW and VS, and S is the area of the 2D elastoplastic fault zone. For all the cases shown in Figure-5c, there is an initial increase of plastic deformation while the potency is small. This indicates plasticity accumulation when the fault is locked prior to any seismic events. When fault slip occurs, both potency and plastic deformation increases but the increment of plastic deformation is relatively lower. For the cases shown in Fig. 5c, the ratio between plastic deformation and potency varies over an order of magnitude ranging from ~ 0.1 for $\sigma_y = 36$ MPa to ~ 3.5 for $\sigma_y = 32$ MPa.

For the same amount of potency, plastic deformation is higher with lower yield strength. The pattern of slip with clustered seismic events ($\sigma_y = 36$ MPa, shown in Figs. 3, 5) is associated with relatively lower plastic deformation to potency ratio (~ 0.1). However, fault slip involving slow slip and partial ruptures spreading over the fault ($\sigma_y = 33.5$ MPa, shown in Figs. 3, 5) correspond to higher ratios of plastic deformation to potency (~ 0.5). Local-

ized seismic event and slow slip in otherwise locked fault ($\sigma_y = 32.5$ MPa, $\sigma_y = 32$ MPa shown in Figs. 3, 5) corresponds to relatively higher plastic deformation to potency ratio (>1). In these limits of low yield strength, more deformation is distributed in the bulk than localized as slip on the fault surface.

Figure 5d shows the ratio of plastic dissipation relative to total dissipation. Total dissipation is the sum of plastic dissipation (PW) and frictional dissipation (FW). Here, frictional dissipation is computed over the region of the fault used to compute the potency. This region includes the VW patch as well as the transition regions between the VW and VS patches. That is, we do not account for frictional dissipation due to slip in the VS region which conforms to the plate loading. Contribution of plastic dissipation is higher with lower yield strength. On one hand, for the case of $\sigma_y = 32$ MPa, generating slow slip events, plastic dissipation is around 80% of the total dissipation. On the other hand, clustered seismic events with $\sigma_y = 36$ MPa is associated with much lower plastic dissipation ($\sim 10\%$ of total dissipation). The decrease in the ratio of plastic to total dissipation is a result of less off-fault plastic deformation and corresponds to higher frictional dissip-

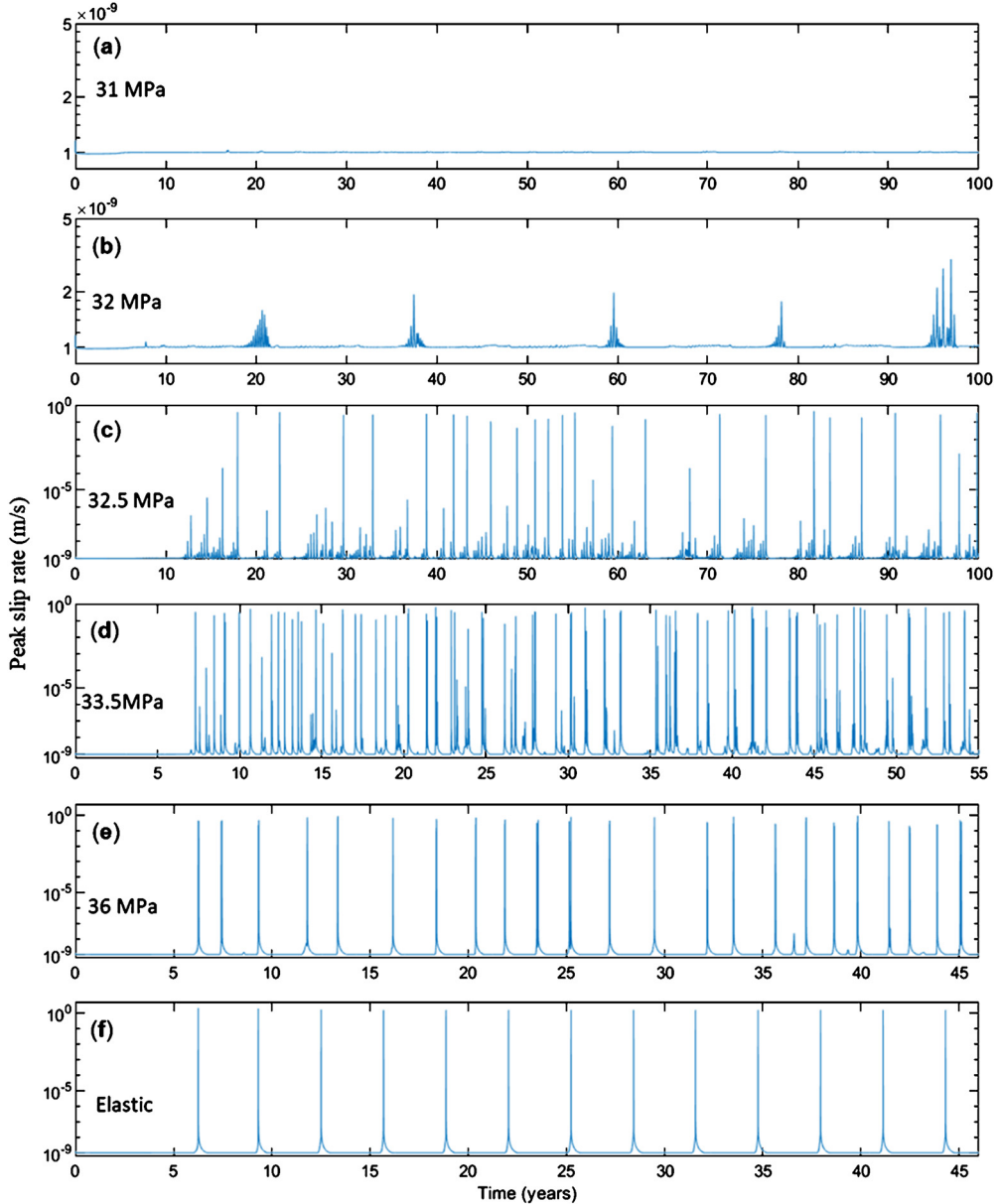


Fig. 4. History of peak slip rate for 2D continuum simulations with different yield strengths (a-e). The elastic reference case is generating periodic pattern is shown in f. Peak slip rate remains close to the plate rate for locked fault with yield strength 31 MPa as shown in a. However, this peak slip rate is limited to the VS region. The slip rate in the VW region drops to 10^{-15} m/s. (b) Slow slip events with 32 MPa. (c) Localized seismic events and preceding slow slip events with 32.5 MPa. (d) Irregular pattern including slow slip and partial rupture with 33.5 MPa. (e) Aperiodic sequence with clustering of seismicity for higher yield strength.

tion through fault slip in large and fast seismic events. Higher off-fault deformation and smaller on-fault slip leads to increased off-fault dissipation. Mia et al. (2022), showed that even if the contribution of plasticity to the energy budget is small, it may still play a significant role in regulating the spatio-temporal clustering of seismic events through limiting the stress concentration ahead of the rupture tip and facilitating rupture arrest. Here, we additionally show that if the energy dissipation is dominated by off-fault plastic dissipation, which happens for lower yield strength, fault-spanning events cannot occur, and slip becomes progressively slower. Specifically, we observe that irregular partial ruptures, slow slip, repeaters, and even complete locking of the VW patch emerge in the limit of low yield strength and increased off-fault plastic dissipation irrespective of fault length. This further suggests that plastic dissipation should be low (less than 10%) compared to total dissipation, for large fault spanning events to occur.

4. Discussion

In this work, we showed, using a simple elastoplastic spring block model, that spring stiffness, even when lower than the critical value for instability predicted by elastic analysis, may not facilitate stick-slip instability if the yield strength is low enough. Since stiffness is inversely proportional to length, this finding suggests that not all perturbations with wavelength greater than the nucleation length are unstable. Rather the maximum wavelength that is unstable may vary depending on yield strength. This implies, for some parameter regime in the presence of off-fault plasticity, that only partial ruptures may exist and that these ruptures cannot grow to become fault spanning events. Similar patterns are observed in continuum 2D anti-plane simulations with different values of yield strength. The rich slip patterns observed in the continuum model include locked fault, slow slip events, localized sequence of seismic event and irregular patterns with partial

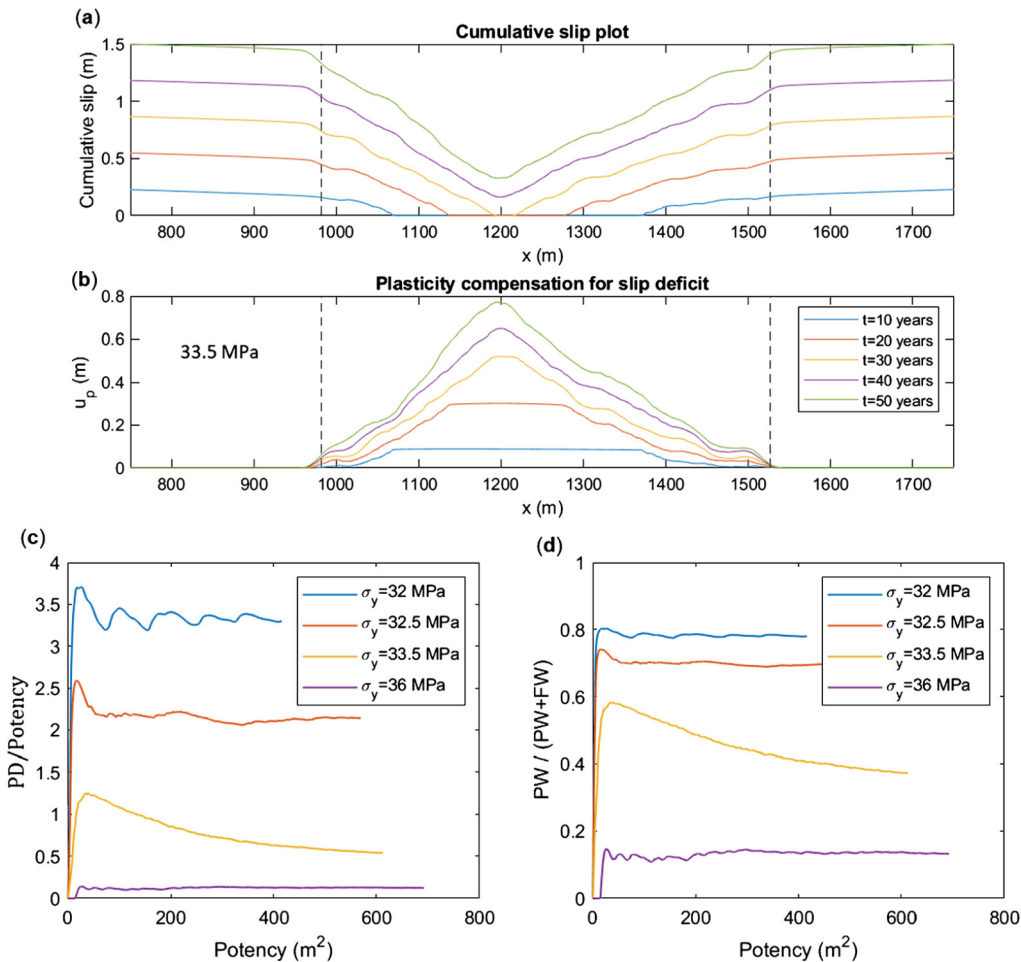


Fig. 5. Plasticity compensation for slip deficit and partitioning of deformation as well as energy dissipation between the bulk and the fault. (a) Cumulative slip is plotted at an interval of 10 years (for $\sigma_y = 33.5$ MPa). (b) Off-fault plastic deformation obtained from integrating the plastic strain in lateral direction is plotted along the fault in the same interval of cumulative slip plot (for $\sigma_y = 33.5$ MPa). The region within the two vertical dashed lines corresponds to the fault section with velocity weakening friction. The extent of locked region subsequently shrinks with increased slip. Plasticity compensation is higher in the region where slip accumulation is lower. (c) Relative contribution of on-fault slip and off-fault plastic deformation. Potency is computed by integrating slip, Potency (t) = $\int_0^{L_f} d(x, t) dx$ and plastic deformation is computed from integrating the plastic strain over the domain, $PD(t) = \int_S \gamma(x, y, t) dS$. Lower yield strength corresponds to higher amount of plastic deformation. (d) Plot of plastic energy dissipation (PW) relative to total dissipation. FW is the frictional dissipation computed over the velocity weakening patch and the transition region. Higher percentage of plastic dissipation is associated with lower yield strength generating slow slip.

ruptures spreading over the fault. Neither frictional heterogeneity nor pore pressure perturbation is introduced here. Only the bulk strength is acting as the controlling factor in modulating the slip pattern.

In a characteristic seismic cycle, VS patch accumulates slip during the interseismic period and VW patch catches up with seismic slip accumulation. However, when the bulk strength is relatively low, seismic events are rare or spatially limited with partial ruptures. This results in slip deficit prevailing throughout the seismic cycle. We found that off-fault plastic deformation compensates for the slip deficit in this case. For sufficiently low bulk strength, fault may remain locked without generating seismic events while off-fault bulk accommodates the deformation through plastic deformation. This is also analogous to the spring slider results where plastic deformation in the spring resists and even, in some cases, prevents the sliding of the block. Relative amount of off-fault plastic deformation and on-fault slip is associated with the spectrum of slip from clustered fast slip to a mixture of fast and slow slip as the yield strength decreases. Inelastic dissipation must remain low for fast fault large events to exist.

We note that large amount of shallow off-fault deformation, exceeding 80% of the total surface deformation (i.e., 4 times the on-fault slip) has been reported around some faults recently by Li

et al. (2022). They hypothesized that the large amount of off-fault deformation may include some elastic deformation. The determination of the extent of inelastic off-fault deformation would be possible if additional data from seismic reflection was available. The plastic strain in our simulation is limited to a narrow region close to the fault (Supplementary Figure-S4). If this holds true for off-fault plasticity accumulation in natural fault zones, particularly at depth, it may be difficult to distinguish between on-fault and off-fault deformation from field observations specially from satellite measurements as there are limitations on high resolution measurements of off-fault deformation (Antoine et al., 2021). This partitioning of deformation is, however, important to quantify as accumulation of off-fault plasticity may have implications for fault weakening. As plastic deformation involves dissipation over narrow but finite region, it can influence the heat diffusion and constrain the rise of temperature associated with slip localization into an extremely thin surface in an otherwise elastic medium (Rice, 2006). This may contribute to understanding the scarcity of fault zone melting in some field observations. However, since most of the plastic dissipation is still in the form of heat, we do not think that off-fault plasticity resolves the heat flow anomaly.

Slow slip events recorded in some field observations show a wide range of durations in the scale of days to months, and large

earthquakes have been found after the migration of slow slip events and small earthquakes (Ito et al., 2013; Ruiz, 2014; Obara and Kato, 2016). The coexistence of slow slip events and small earthquakes in subduction zone has also been reported by Ito et al., 2007. In our simulation, fault slip accompanied by a mixture of seismic events with partial ruptures and slow slip events are observed. Some of the slow slip events show spatial migration over the seismogenic patch with duration reaching the scale of months. We observe emergence of spectrum of slip by simulating different cases with small difference in yield strength. In natural fault zone, off-fault bulk property (for example, yield strength) may vary spatially and evolve with time. Since yield strength depends on effective normal stress, physical process like fluid pressure perturbation may alter the yield strength independent of fault strength alteration depending on the hydraulic properties in the fault core relative to the fault zone. Healing of damaged fault zone may also contribute to the evolution of yield strength. Consequently, a fault may host different patterns of slip switching from fast seismic rupture to slow aseismic slip when yield strength transiently decreases.

The localized seismic events observed in our continuum simulations, at the boundary of the VW and VS regions, is analogous to repeating microseismicity model presented in Sammis and Rice (2001) but some differences exist. The similarity is that the location of the seismic events is near the transition between creeping asperity (VS patch) and seismogenic locked asperity (VW patch). The slip deficit in their model is compensated by occasional full-fault spanning events whereas the slip deficit in our simulations is compensated by off-fault plastic deformation. Also, in our simulations, there are slow slip events in between the seismic events.

Numerical modeling of fault damage zone (Nie and Barbot, 2022; Thakur and Huang, 2021; Abdelmeguid et al., 2019; Kaneko et al., 2011) with a layer of reduced elastic modulus shows increased slip rate, and a range of slip pattern depending on the width and the contrast of elastic modulus. A more compliant layer near the fault corresponds to generate more intense rupture. On the other hand, plasticity as a dissipative mechanism influences the rupture characteristics resulting in reduced slip rate and rupture speed (Templeton and Rice, 2008; Viesca et al., 2008; Dunham et al., 2011a, 2011b; Gabriel et al., 2013). Furthermore, in contrast to elastic bulk, plasticity limits the stress concentration ahead of the rupture tip. It acts as a barrier to rupture propagation and may result in spatial segmentation and temporal clustering (Mia et al., 2022). In this study, we model elastoplastic deformation of off-fault bulk keeping the elastic modulus constant throughout. Total deformation is partitioned into fault slip and off-fault plastic deformation. Depending on the bulk yield strength and frictional strength, the contribution of plasticity may compensate for a larger amount of the total deformation and reduce fault slip leading to emergence of a variety of slip patterns from fast to slow. However, fault zone inelasticity may include processes that go beyond plastic dissipation such as co-seismic degradation of the elastic moduli and their inter-seismic healing. The time-dependent modulation of the fault zone elastic properties may further enrich the observed slip complexity, enhance seismic radiation, and expand the conditions for generation of slow slip. Incorporation of off-fault plasticity coupled with damage rheology in SEAS is a focus of a future investigation.

In this model, we consider the frictional parameters like reference friction coefficient, direct effect, and state evolution coefficient to remain stationary. However, frictional parameters may evolve with coseismic deformation (Kaproth and Marone, 2013; Im et al., 2020) which may get pronounced with off-fault damage or plasticity accumulation. Investigating the interplay between evolving fault friction as well as degradation and subsequent healing of fault zone material warrants future study. Fault zone geometric

complexity including nonplanar faults, and interaction of multiple faults in presence of off-fault material non-linearity, is planned as future study. Furthermore, evolution of pore pressure associated with volumetric deformation of the fault zone needs to be considered for its vast implications on the evolution of strength and deformation in fluid-saturated fault zones.

CRediT authorship contribution statement

Md Shumon Mia: Conceptualization, Formal analysis, Methodology, Software, Visualization, Writing – original draft, Writing – review & editing. **Mohamed Abdelmeguid:** Conceptualization, Formal analysis, Methodology, Software, Visualization, Writing – review & editing. **Ahmed E. Elbanna:** Conceptualization, Formal analysis, Funding acquisition, Methodology, Software, Supervision, Visualization, Writing – original draft, Writing – review & editing.

Declaration of competing interest

The authors declare that they have no known competing financial interests or personal relationships that could have appeared to influence the work reported in this paper.

Data availability

Data generated from the numerical simulations are uploaded on an open access repository (<https://doi.org/10.5281/zenodo.7718768>).

Acknowledgement

The authors acknowledge support from the Southern California Earthquake Center through a collaborative agreement between NSF, Grant Number: EAR0529922 and USGS, Grant Number: 07HQAG0008 and the National Science Foundation CAREER award No. 1753249 for modeling complex fault zone structures. This material is also based upon work partially supported by the Department of Energy under Award Number DE-FE0031685 to investigate spatio-temporal complexity of induced earthquakes. The authors are also grateful for the insightful comments from two anonymous reviewers, which helped improve the manuscript.

Appendix A. Supplementary material

Supplementary material related to this article can be found online at <https://doi.org/10.1016/j.epsl.2023.118310>.

References

- Abdelmeguid, M., Ma, X., Elbanna, A., 2019. A novel hybrid finite element-spectral boundary integral scheme for modeling earthquake cycles: application to rate and state faults with low-velocity zones. *J. Geophys. Res., Solid Earth* 124 (12), 12854–12881. <https://doi.org/10.1029/2019JB018036>.
- Abdelmeguid, M., Elbanna, A., 2022a. Sequences of seismic and aseismic slip on bimaterial faults show dominant rupture asymmetry and potential for elevated seismic hazard. *Earth Planet. Sci. Lett.* 593. <https://doi.org/10.1016/j.epsl.2022.117648>.
- Abdelmeguid, M., Elbanna, A., 2022b. Modeling sequences of earthquakes and aseismic slip (SEAS) in elasto-plastic fault zones with a hybrid finite element spectral boundary integral scheme. *J. Geophys. Res., Solid Earth* 127 (12). <https://doi.org/10.1029/2022JB024548>.
- Allison, K.L., Dunham, E.M., 2021. Influence of shear heating and thermomechanical coupling on earthquake sequences and the brittle-ductile transition. *J. Geophys. Res., Solid Earth* 126 (6). <https://doi.org/10.1029/2020JB021394>.
- Ampuero, J.P., Rubin, A.M., 2008. Earthquake nucleation on rate and state faults – aging and slip laws. *J. Geophys. Res., Solid Earth* 113 (1). <https://doi.org/10.1029/2007JB005082>.
- Antoine, S.L., Klinger, Y., Delorme, A., Wang, K., Bürgmann, R., Gold, R.D., 2021. Diffuse deformation and surface faulting distribution from submetric image correlation along the 2019 ridgecrest, California, ruptures. *Bull. Seismol. Soc. Am.* 111 (5), 2275–2302. <https://doi.org/10.1785/0120210036>.

Avouac, J.P., 2015. From geodetic imaging of seismic and aseismic fault slip to dynamic modeling of the seismic cycle. *Annu. Rev. Earth Planet. Sci.* 43, 233–271. <https://doi.org/10.1146/annurev-earth-060614-105302>.

Barbot, S., Lapusta, N., Avouac, J.-P., 2012. Under the hood of the earthquake machine: toward predictive modeling of the seismic cycle. *Science* 336 (6082), 707–710. <https://doi.org/10.1126/science.1218796>.

Barbot, S., 2019. Slow-slip, slow earthquakes, period-two cycles, full and partial ruptures, and deterministic chaos in a single asperity fault. *Tectonophysics* 768. <https://doi.org/10.1016/j.tecto.2019.228171>.

Bedford, J.D., Faulkner, D.R., Lapusta, N., 2022. Fault rock heterogeneity can produce fault weakness and reduce fault stability. *Nat. Commun.* 13 (1). <https://doi.org/10.1038/s41467-022-27998-2>.

Ben-Zion, Y., Rice, J.R., 1997. Dynamic simulations of slip on a smooth fault in an elastic solid. *J. Geophys. Res., Solid Earth* 102 (B8), 17771–17784.

Ben-Zion, Y., Rice, J.R., 1993. Earthquake failure sequences along a cellular fault zone in a three-dimensional elastic solid containing asperity and nonasperity regions. *J. Geophys. Res.* 98 (B8). <https://doi.org/10.1029/93jb01096>.

Ben-Zion, Y., Sammis, C.G., 2003. Characterization of fault zones. In: *Pure Appl. Geophys.* 160.

Beroza, G.C., Ide, S., 2011. Slow earthquakes and nonvolcanic tremor. *Annu. Rev. Earth Planet. Sci.* 39, 271–296. <https://doi.org/10.1146/annurev-earth-040809-152531>.

Bürgmann, R., 2018. The geophysics, geology and mechanics of slow fault slip. *Earth Planet. Sci. Lett.* 495, 112–134. <https://doi.org/10.1016/j.epsl.2018.04.062>.

Cattania, C., 2019. Complex earthquake sequences on simple faults. *Geophys. Res. Lett.* 46 (17–18), 10384–10393. <https://doi.org/10.1029/2019GL083628>.

Chen, T., Lapusta, N., 2009. Scaling of small repeating earthquakes explained by interaction of seismic and aseismic slip in a rate and state fault model. *J. Geophys. Res.* 114, 1311. <https://doi.org/10.1029/2008JB005749>.

Chen, Y., Liu, M., Luo, G., 2020. Complex temporal patterns of large earthquakes: Devil's staircases. *Bull. Seismol. Soc. Am.* 110 (3), 1064–1076. <https://doi.org/10.1785/0120190148>.

Collettini, C., Barchi, M.R., de Paola, N., Trippetta, F., Tinti, E., 2022. Rock and fault rheology explain differences between on-fault and distributed seismicity. *Nat. Commun.* 13 (1). <https://doi.org/10.1038/s41467-022-33373-y>.

Collettini, C., Tesei, T., Scuderi, M.M., Carpenter, B.M., Viti, C., 2019. Beyond Byerlee friction, weak faults and implications for slip behavior. *Earth Planet. Sci. Lett.* 519, 245–263. <https://doi.org/10.1016/j.epsl.2019.05.011>.

Dieterich, J.H., 1978. Time-dependent friction and the mechanics of stick-slip. *Pure Appl. Geophys.* 116 (4–5), 790–806.

Dieterich, J.H., 1979. Modeling of rock friction: 1. Experimental results and constitutive equations. *J. Geophys. Res., Solid Earth* 84 (B5), 2161–2168.

Dragert, H., Wang, K., James, T.S., 2001. A silent slip event on the deeper Cascadia subduction interface. *Science* 292 (5521), 1525–1528. <https://doi.org/10.1126/science.1060152>.

Dunham, E.M., Belanger, D., Cong, L., Kozdon, J.E., 2011a. Earthquake ruptures with strongly rate-weakening friction and off-fault plasticity, part 1: planar faults. *Bull. Seismol. Soc. Am.* 101 (5), 2296–2307.

Dunham, E.M., Belanger, D., Cong, L., Kozdon, J.E., 2011b. Earthquake ruptures with strongly rate-weakening friction and off-fault plasticity, part 2: nonplanar faults. *Bull. Seismol. Soc. Am.* 101 (5), 2308–2322.

Erickson, B.A., Dunham, E.M., Khosrovifar, A., 2017. A finite difference method for off-fault plasticity throughout the earthquake cycle. *J. Mech. Phys. Solids* 109, 50–77.

Erickson, B.A., Jiang, J., Lambert, V., Barbot, S.D., Abdelmeguid, M., Almquist, M., Ampuero, J.-P., Ando, R., Cattania, C., Chen, A., Dal Zilio, L., Deng, S., Dunham, E.M., Elbanna, A.E., Gabriel, A.-A., Harvey, T.W., Huang, Y., Kaneko, Y., Kozdon, J.E., Yang, Y., 2023. Incorporating full elastodynamic effects and dipping fault geometries in community code verification exercises for simulations of earthquake sequences and aseismic slip (SEAS). *Bull. Seismol. Soc. Am.* <https://doi.org/10.1785/0120220066>.

French, M.E., Zhu, W., 2017. Slow fault propagation in serpentinite under conditions of high pore fluid pressure. *Earth Planet. Sci. Lett.* 473, 131–140. <https://doi.org/10.1016/j.epsl.2017.06.009>.

Fagereng, Å., Sibson, R.H., 2010. Mélange rheology and seismic style. *Geology* 38 (8), 751–754. <https://doi.org/10.1130/G30868.1>.

Gabriel, A.A., Ampuero, J.P., Dalguer, L.A., Mai, P.M., 2013. Source properties of dynamic rupture pulses with off-fault plasticity. *J. Geophys. Res., Solid Earth* 118 (8), 4117–4126.

Goswami, A., Barbot, S., 2018. Slow-slip events in semi-brittle serpentinite fault zones. *Sci. Rep.* 8 (1). <https://doi.org/10.1038/s41598-018-24637-z>.

Heki, K., Kataoka, T., 2008. On the biannually repeating slow-slip events at the Ryukyu Trench, southwestern Japan. *J. Geophys. Res., Solid Earth* 113 (11). <https://doi.org/10.1029/2008JB005739>.

Im, K., Saffer, D., Marone, C., Avouac, J.P., 2020. Slip-rate-dependent friction as a universal mechanism for slow slip events. *Nat. Geosci.* 13 (10), 705–710. <https://doi.org/10.1038/s41561-020-0627-9>.

Ito, Y., Hino, R., Kido, M., Fujimoto, H., Osada, Y., Inazu, D., Ohta, Y., Iinuma, T., Ohzono, M., Miura, S., Mishina, M., Suzuki, K., Tsuji, T., Ashi, J., 2013. Episodic slow slip events in the Japan subduction zone before the 2011 Tohoku-Oki earthquake. *Tectonophysics* 600, 14–26. <https://doi.org/10.1016/j.tecto.2012.08.022>.

Ito, Y., Obara, K., Shiomi, K., Sekine, S., Hirose, H., 2007. Slow earthquakes coincident with episodic tremors and slow slip events. *Science* 315 (5811), 503–506. <https://doi.org/10.1126/science.1134454>.

Jiang, J., Erickson, B.A., Lambert, V.R., Ampuero, J.P., Ando, R., Barbot, S.D., Cattania, C., Zilio, L.D., Duan, B., Dunham, E.M., Gabriel, A.A., Lapusta, N., Li, D., Li, M., Liu, D., Liu, Y., Ozawa, S., Pranger, C., van Dinther, Y., 2022. Community-driven code comparisons for three-dimensional dynamic modeling of sequences of earthquakes and aseismic slip. *J. Geophys. Res., Solid Earth* 127 (3). <https://doi.org/10.1029/2021JB023519>.

Kaproth, B.M., Marone, C., 2013. Slow earthquakes, preseismic velocity changes, and the origin of slow frictional stick-slip. *Science* 341 (6151), 1229–1232. <https://doi.org/10.1126/science.1239577>.

Kaneko, Y., Avouac, J.P., Lapusta, N., 2010. Towards inferring earthquake patterns from geodetic observations of interseismic coupling. *Nat. Geosci.* 3 (5), 363–369. <https://doi.org/10.1038/geo843>.

Kaneko, Y., Ampuero, J.P., Lapusta, N., 2011. Spectral-element simulations of long-term fault slip: effect of low-rigidity layers on earthquake-cycle dynamics. *J. Geophys. Res., Solid Earth* 116 (B10).

Lapusta, N., Rice, J.R., Ben-Zion, Y., Zheng, G., 2000. Elastodynamic analysis for slow tectonic loading with spontaneous rupture episodes on faults with rate- and state-dependent friction. *J. Geophys. Res., Solid Earth* 105 (B10), 23765–23789. <https://doi.org/10.1029/2000jb002050>.

Leeman, J.R., Saffer, D.M., Scuderi, M.M., Marone, C., 2016. Laboratory observations of slow earthquakes and the spectrum of tectonic fault slip modes. *Nat. Commun.* 7 (1), 11104.

Lewis, M.A., Ben-Zion, Y., 2010. Diversity of fault zone damage and trapping structures in the parkfield section of the San Andreas fault from comprehensive analysis of near fault seismograms. *Geophys. J. Int.* 183 (3), 1579–1595. <https://doi.org/10.1111/j.1365-246X.2010.04816.x>.

Li, C., Li, T., Shan, X., Zhang, G., 2022. Extremely large off-fault deformation during the 2021 Mw 7.4 Madou, Tibetan Plateau, Earthquake. *Seismol. Res. Lett.* <https://doi.org/10.1785/0220220139>.

Liu, Y., Rice, J.R., 2007. Spontaneous and triggered aseismic deformation transients in a subduction fault model. *J. Geophys. Res., Solid Earth* 112 (9). <https://doi.org/10.1029/2007JB004930>.

Mia, M.S., Abdelmeguid, M., Elbanna, A.E., 2022. Spatio-temporal clustering of seismicity enabled by off-fault plasticity. *Geophys. Res. Lett.* 49, e2021GL097601. <https://doi.org/10.1029/2021GL097601>.

Mitchell, T.M., Faulkner, D.R., 2009. The nature and origin of off-fault damage surrounding strike-slip fault zones with a wide range of displacements: a field study from the Atacama fault system, northern Chile. *J. Struct. Geol.* 31 (8), 802–816. <https://doi.org/10.1016/j.jsg.2009.05.002>.

Miyake, Y., Noda, H., 2019. Fully dynamic earthquake sequence simulation of a fault in a viscoelastic medium using a spectral boundary integral equation method: does interseismic stress relaxation promote aseismic transients? *Earth Planets Space* 71 (1), 1–12.

Nie, S., Barbot, S., 2022. Rupture styles linked to recurrence patterns in seismic cycles with a compliant fault zone. *Earth Planet. Sci. Lett.* 591. <https://doi.org/10.1016/j.epsl.2022.117593>.

Nakata, R., Ando, R., Hori, T., Ide, S., 2011. Generation mechanism of slow earthquakes: numerical analysis based on a dynamic model with brittle-ductile mixed fault heterogeneity. *J. Geophys. Res., Solid Earth* 116 (8). <https://doi.org/10.1029/2010JB008188>.

Noda, H., Lapusta, N., 2013. Stable creeping fault segments can become destructive as a result of dynamic weakening. *Nature* 493 (7433), 518–521. <https://doi.org/10.1038/nature11703>.

Obara, K., Kato, A., 2016. Connecting slow earthquakes to huge earthquakes. *Science* 353 (6296), 253–257. <https://doi.org/10.1126/science.aaf1512>.

Radiguet, M., Cotton, F., Vergnolle, M., Campillo, M., Walpersdorf, A., Cotte, N., Kostoglodov, V., 2012. Slow slip events and strain accumulation in the Guerrero gap Mexico. *J. Geophys. Res., Solid Earth* 117 (4). <https://doi.org/10.1029/2011JB008801>.

Ranjith, K., Rice, J.R., 1999. Stability of quasi-static slip in a single degree of freedom elastic system with rate and state dependent friction. *J. Mech. Phys. Solids* 47 (6), 1207–1218. [https://doi.org/10.1016/S0022-5096\(98\)00113-6](https://doi.org/10.1016/S0022-5096(98)00113-6).

Rice, J.R., 2006. Heating and weakening of faults during earthquake slip. *J. Geophys. Res., Solid Earth* 111 (5). <https://doi.org/10.1029/2005JB004006>.

Rice, J.R., Ruina, A.L., 1983. Stability of steady frictional slipping. *J. Appl. Mech.* 50 (2), 343–349. <https://doi.org/10.1115/1.3167042>.

Rice, J.R., Lapusta, N., Ranjith, K., 2001. Rate and state dependent friction and the stability of sliding between elastically deformable solids. *J. Mech. Phys. Solids* 49 (9), 1865–1898. [https://doi.org/10.1016/S0022-5096\(01\)00042-4](https://doi.org/10.1016/S0022-5096(01)00042-4).

Ross, Z.E., Cochran, E.S., Trugman, D.T., Smith, J.D., 2020. 3D fault architecture controls the dynamism of earthquake swarms. *Science* 368 (6497), 1357–1361. <https://doi.org/10.1126/science.abb0779>.

Ruina, A., 1983. Slip instability and state variable friction laws. *J. Geophys. Res., Solid Earth* 88 (B12), 10359–10370.

Ruiz, S., Metois, M., Fuenzalida, A., Ruiz, J., Leyton, F., Grandin, R., Campos, J., 2014. Intense foreshocks and a slow slip event preceded the 2014 Iquique Mw

8.1 earthquake. *Science* 345 (6201), 1165–1169. <https://doi.org/10.1126/science.1256074>.

Sammis, C.G., Rice, J.R., 2001. Repeating earthquakes as low-stress-drop events at a border between locked and creeping fault patches. *Bull. Seismol. Soc. Am.* 91 (3), 532–537. <https://doi.org/10.1785/0120000075>.

Scuderi, M.M., Marone, C., Tinti, E., Di Stefano, G., Collettini, C., 2016. Precursory changes in seismic velocity for the spectrum of earthquake failure modes. *Nat. Geosci.* 9 (9), 695–700. <https://doi.org/10.1038/ngeo2775>.

Segall, P., Rubin, A.M., Bradley, A.M., Rice, J.R., 2010. Dilatant strengthening as a mechanism for slow slip events. *J. Geophys. Res., Solid Earth* 115 (12). <https://doi.org/10.1029/2010JB007449>.

Skarbek, R.M., Rempel, A.W., Schmidt, D.A., 2012. Geologic heterogeneity can produce aseismic slip transients. *Geophys. Res. Lett.* 39 (21). <https://doi.org/10.1029/2012GL053762>.

Templeton, E.L., Rice, J.R., 2008. Off-fault plasticity and earthquake rupture dynamics: 1. Dry materials or neglect of fluid pressure changes. *J. Geophys. Res., Solid Earth* 113 (B9).

Thakur, P., Huang, Y., Kaneko, Y., 2020. Effects of low-velocity fault damage zones on long-term earthquake behaviors on mature strike-slip faults. *J. Geophys. Res., Solid Earth* 125 (8), e2020JB019587.

Thakur, P., Huang, Y., 2021. Influence of fault zone maturity on fully dynamic earthquake cycles. *Geophys. Res. Lett.* 48 (17), e2021GL094679.

Tong, X., Lavier, L.L., 2018. Simulation of slip transients and earthquakes in finite thickness shear zones with a plastic formulation. *Nat. Commun.* 9 (1). <https://doi.org/10.1038/s41467-018-06390-z>.

Viesca, R.C., Templeton, E.L., Rice, J.R., 2008. Off-fault plasticity and earthquake rupture dynamics: 2. Effects of fluid saturation. *J. Geophys. Res., Solid Earth* 113 (B9).

Wu, B., 2021. Explaining Slow Earthquake Phenomena with a Frictional-Viscous Faulting Model (Doctoral Dissertation). University of California, Riverside.